Cell Stem Cell, Volume *27*

Supplemental Information

Human Pluripotent Stem Cell-Derived Neural Cells and Brain Organoids Reveal SARS-CoV-2 Neurotropism Predominates in Choroid Plexus Epithelium

Fadi Jacob, Sarshan R. Pather, Wei-Kai Huang, Feng Zhang, Samuel Zheng Hao Wong, Haowen Zhou, Beatrice Cubitt, Wenqiang Fan, Catherine Z. Chen, Miao Xu, Manisha Pradhan, Daniel Y. Zhang, Wei Zheng, Anne G. Bang, Hongjun Song, Juan Carlos de la Torre, and Guo-li Ming

SUPPLEMENTARY FIGURES

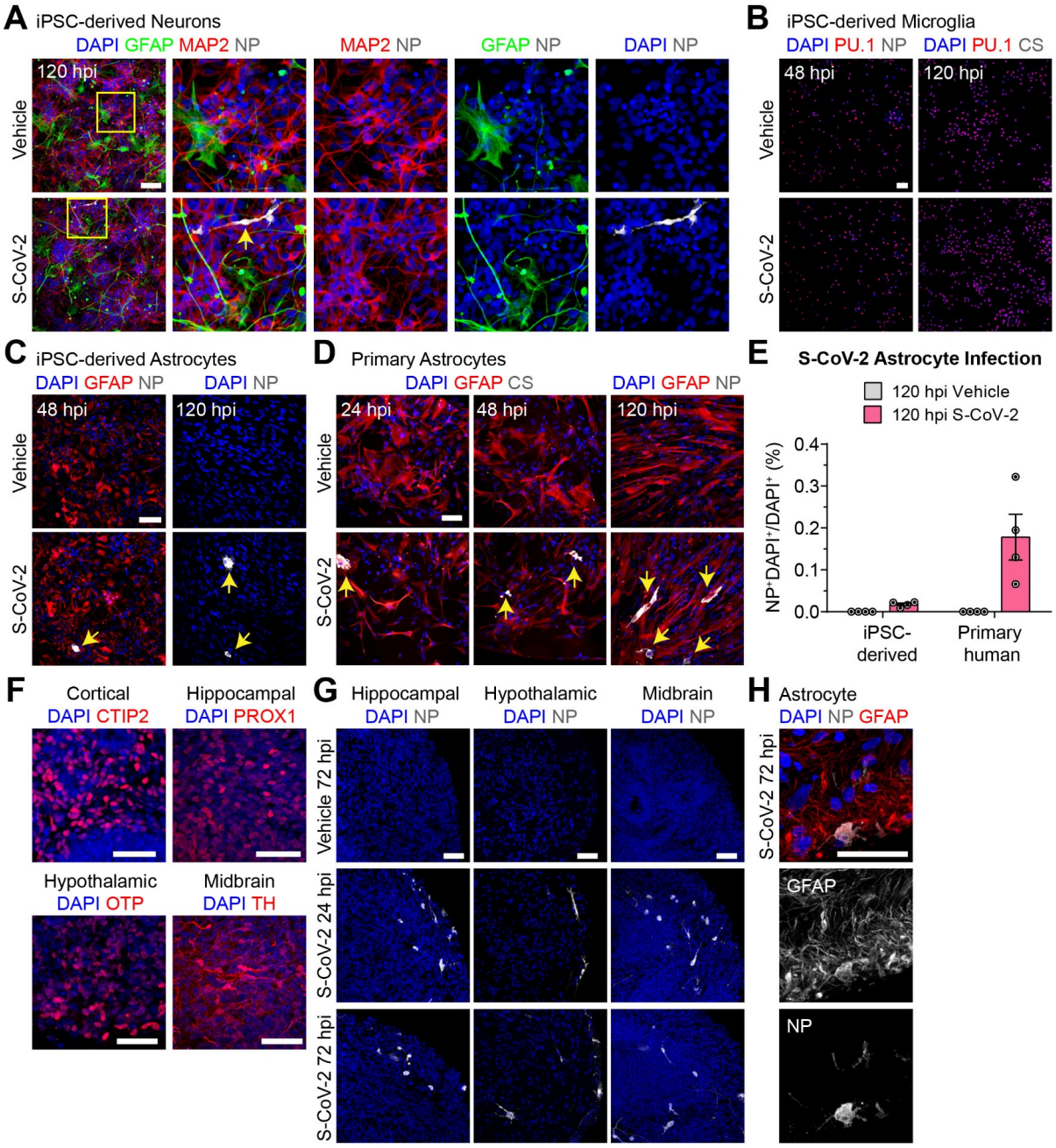

Figure S1. SARS-CoV-2 Neurotropism in hiPSC-derived Monolayer Neural Cultures and Brain Organoids, related to Figure 1

(A) Representative confocal images of fluorescent immunocytochemistry for DAPI, SARS-CoV-2 (S-CoV-2) nucleoprotein (NP), GFAP, and MAP2 in hiPSC-derived cortical neurons plated on hiPSC-derived astrocytes after S-CoV-2 (MOI = 5) or vehicle treatment at 120 hpi. Arrow points to an infected MAP2$^+$ neuron. Scale bar, 50 μm. MOI: multiplicity of infection.

(B) Representative confocal images of fluorescent immunocytochemistry for DAPI, NP or convalescent serum from a patient with COVID-19 (CS), and PU.1 in hiPSC-derived microglia after S-CoV-2 (MOI = 5) or vehicle treatment at 48 and 120 hpi. Scale bar, 50 μm. Note a lack of infected cells at both time points.

(C) Representative confocal images of fluorescent immunocytochemistry for DAPI, NP, and GFAP in hiPSC-derived astrocytes after S-CoV-2 (MOI = 5) or vehicle treatment at 48 and 120 hpi. Scale bar, 50 μm. Arrows point to infected cells.
(D) Representative confocal images of fluorescent immunocytochemistry for DAPI, NP or patient convalescent serum (CS), and GFAP in human primary astrocytes after S-CoV-2 (MOI = 5) or vehicle treatment at 24, 48, and 120 hpi. Scale bar, 50 μm. Arrows point to infected cells.
(E) Quantification of percentages of NP^+DAPI^+ cells among $DAPI^+$ cells in S-CoV-2 (MOI = 5) or vehicle treated hiPSC-derived astrocyte and human primary astrocyte cultures at 120 hpi. Values represent mean ± SEM with individual data points plotted (n = 4 independent wells per condition).
(F) Representative confocal images of fluorescent immunohistology for DAPI and CTIP2, PROX1, OTP, and TH in cortical, hippocampal, hypothalamic, and midbrain organoids, respectively. Scale bars, 50 μm.
(G) Representative confocal images of fluorescent immunohistology for DAPI and NP in hippocampal, hypothalamic, and midbrain organoids derived from a second independent hiPSC line after S-CoV-2 (10^5 FFU) or vehicle treatment at 24 and 72 hpi. Scale bars, 50 μm. FFU: focus forming units.
(H) Representative confocal images of fluorescent immunohistology for DAPI, NP, and GFAP in a hypothalamic organoid after S-CoV-2 treatment (10^5 FFU) at 72 hpi. Scale bar, 50 μm.

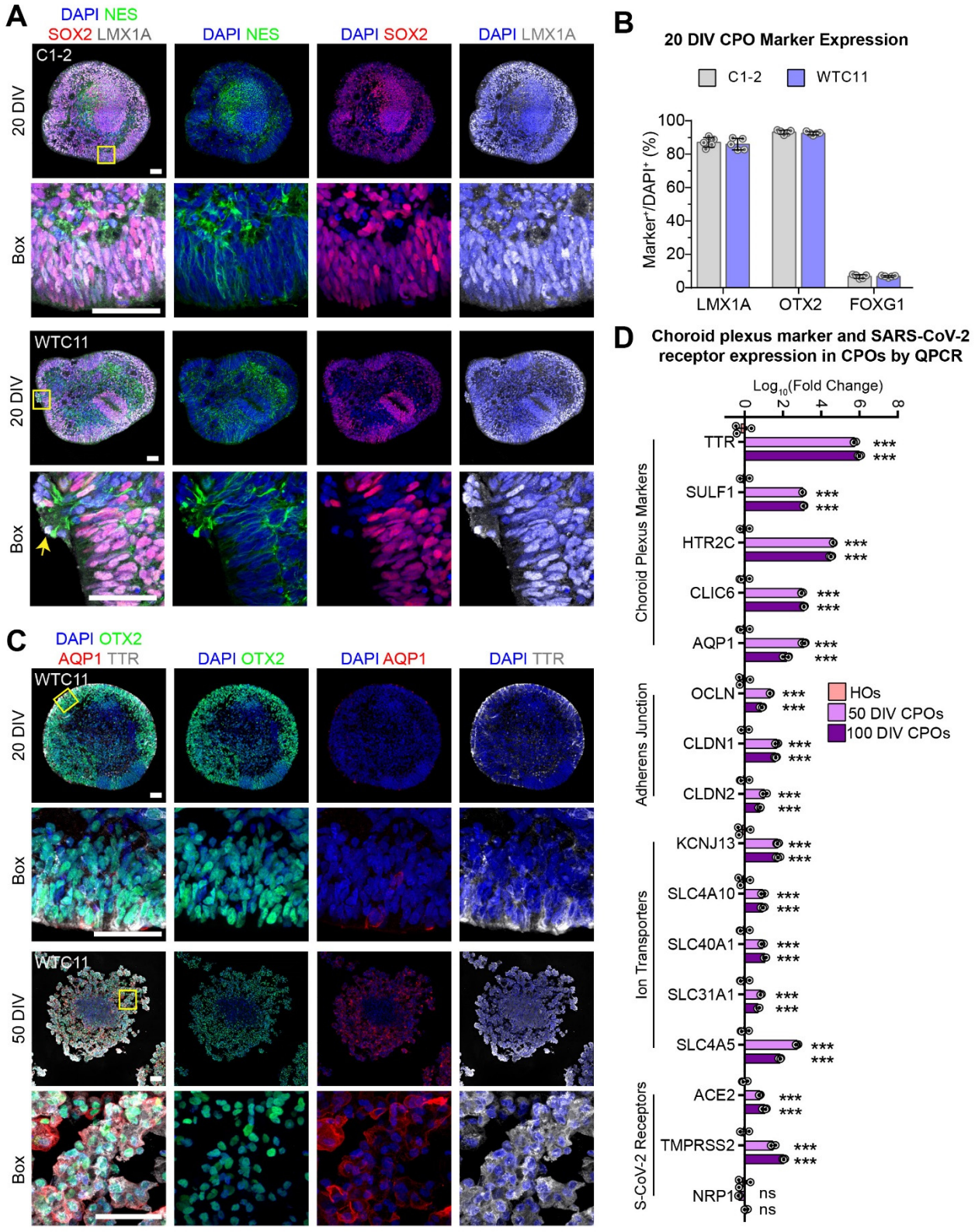

Figure S2. Additional Characterization of hiPSC-derived Choroid Plexus Organoids, related to Figure 2

(A) Representative confocal images of fluorescent immunohistology for DAPI, LMX1A, NESTIN (NES), and SOX2 in 20 DIV CPOs made from C1-2 (top) and WTC11 (bottom) hiPSCs. Images for

the whole organoids are tiled images (top panels for C1-2 and WTC11 iPSC lines). Yellow arrow highlights a region beginning to differentiate into choroid plexus from the neuroepithelium. Scale bars, 50 μm.
(B) Quantification of percentages of $LMX1A^+$, $OTX2^+$, and $FOXG1^+$ cells among $DAPI^+$ cells in 20 DIV CPOs. Values represent mean ± SEM with individual data points plotted (n = 5 organoids per hiPSC line with 3 images per organoid).
(C) Representative confocal images of fluorescent immunohistology for DAPI, OTX2, AQP1, and TTR in 20 and 50 DIV CPOs made from WTC11 hiPSCs. Images for the whole organoids are tiled images (top panels for 20 DIV and 50 DIV). Scale bars, 50 μm.
(D) Quantification of Log_{10}(Fold Change) of choroid plexus signature genes and SARS-CoV-2 receptor genes in 20 DIV hippocampal organoids (HOs), 50 DIV CPOs, and 100 DIV CPOs by QPCR. Data were normalized to that of HOs to calculate the fold change for each gene. Values represent mean ± SEM with individual data points plotted (n = 3 biological replicates for organoids; ***$p < 0.01$; ns, not significant, $p > 0.05$; Fisher's LSD Test).

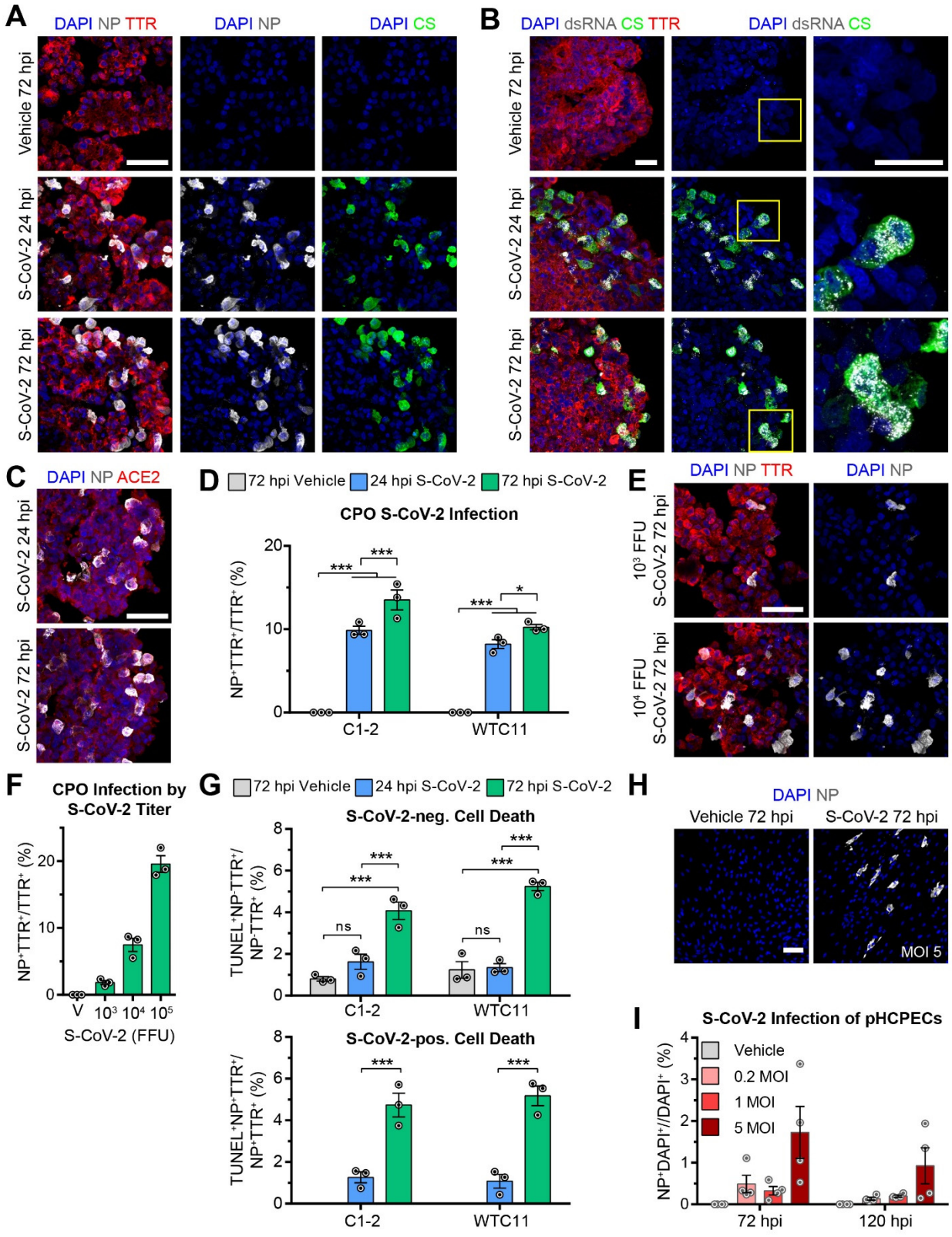

Figure S3. Additional Characterization of SARS-CoV-2 Infected Choroid Plexus Organoids and Infection of Primary Human Choroid Plexus Epithelial Cells, related to Figure 3

(A) Representative confocal images of fluorescent immunohistology for DAPI, SARS-CoV-2 nucleoprotein (NP), patient convalescent serum (CS), and TTR in after S-CoV-2 (10^5 FFU) or vehicle treatment of 67 DIV CPOs made from WTC11 hiPSCs at 24 and 72 hpi. Scale bar, 50 μm.
(B) Representative confocal images of fluorescent immunohistology for DAPI, double-stranded RNA (dsRNA), patient convalescent serum (CS), and TTR after S-CoV-2 (10^5 FFU) or vehicle treatment of 47 DIV CPOs made from WTC11 hiPSCs at 24 and 72 hpi. Boxed regions highlight NP^+ cells containing many dsRNA puncta. Scale bars, 25 μm.
(C) Representative confocal images of fluorescent immunohistology for DAPI, NP, and ACE2 after S-CoV-2 (10^5 FFU) treatment of 47 DIV CPOs made from C1-2 hiPSCs at 24 and 72 hpi. Scale bars, 50 μm.
(D) Quantification of percentages of NP^+TTR^+ cells among TTR^+ cells after S-CoV-2 (10^5 FFU) or vehicle treatment of 47 DIV CPOs at 24 and 72 hpi. Values represent mean ± SEM with individual data points plotted (n = 3 organoids per hiPSC line with 3 images per organoid; *p < 0.05; ***p < 0.001; Fisher's LSD Test).
(E) Representative confocal images of fluorescent immunohistology for DAPI, NP, and TTR after 10^3 or 10^4 FFU S-CoV-2 treatment of 67 DIV CPOs made from C1-2 hiPSCs at 72 hpi. Scale bar, 50 μm.
(F) Quantification of the percentages of NP^+TTR^+ among TTR^+ cells after 10^3, 10^4, or 10^5 FFU S-CoV-2 or vehicle treatment of 70 DIV CPOs made C1-2 hiPSCs at 72 hpi. Values represent mean ± SEM with individual data points plotted (n = 3 organoids per treatment group with 3 images per organoid). Data for 10^5 FFU S-CoV-2 or vehicle treatment (V) at 72 hpi are the same as data plotted in Figure 3B.
(G) Quantification of percentages of $TUNEL^+NP^-TTR^+$ among NP^-TTR^+ cells (top) and $TUNEL^+NP^+TTR^+$ cells among NP^+TTR^+ cells (bottom) after S-CoV-2 (10^5 FFU) or vehicle treatment of 47 DIV CPOs at 24 and 72 hpi. Values represent mean ± SEM with individual data points plotted (n = 3 organoids per treatment group per hiPSC line with 3 images per organoid; ***p < 0.001; ns, not significant, p > 0.05; Fisher's LSD Test).
(H) Representative confocal images of fluorescent immunohistology for DAPI and NP in primary human choroid plexus epithelial cell (pHCPEC) cultures after S-CoV-2 (MOI = 5) or vehicle treatment at 72 hpi. Scale bar, 50 μm.
(I) Quantification of percentages of NP^+DAPI^+ among $DAPI^+$ cells in pHCPEC cultures after S-CoV-2 or vehicle treatment using different MOIs at 72 and 120 hpi. Values represent mean ± SEM with individual data points plotted (n = 4 individual wells).

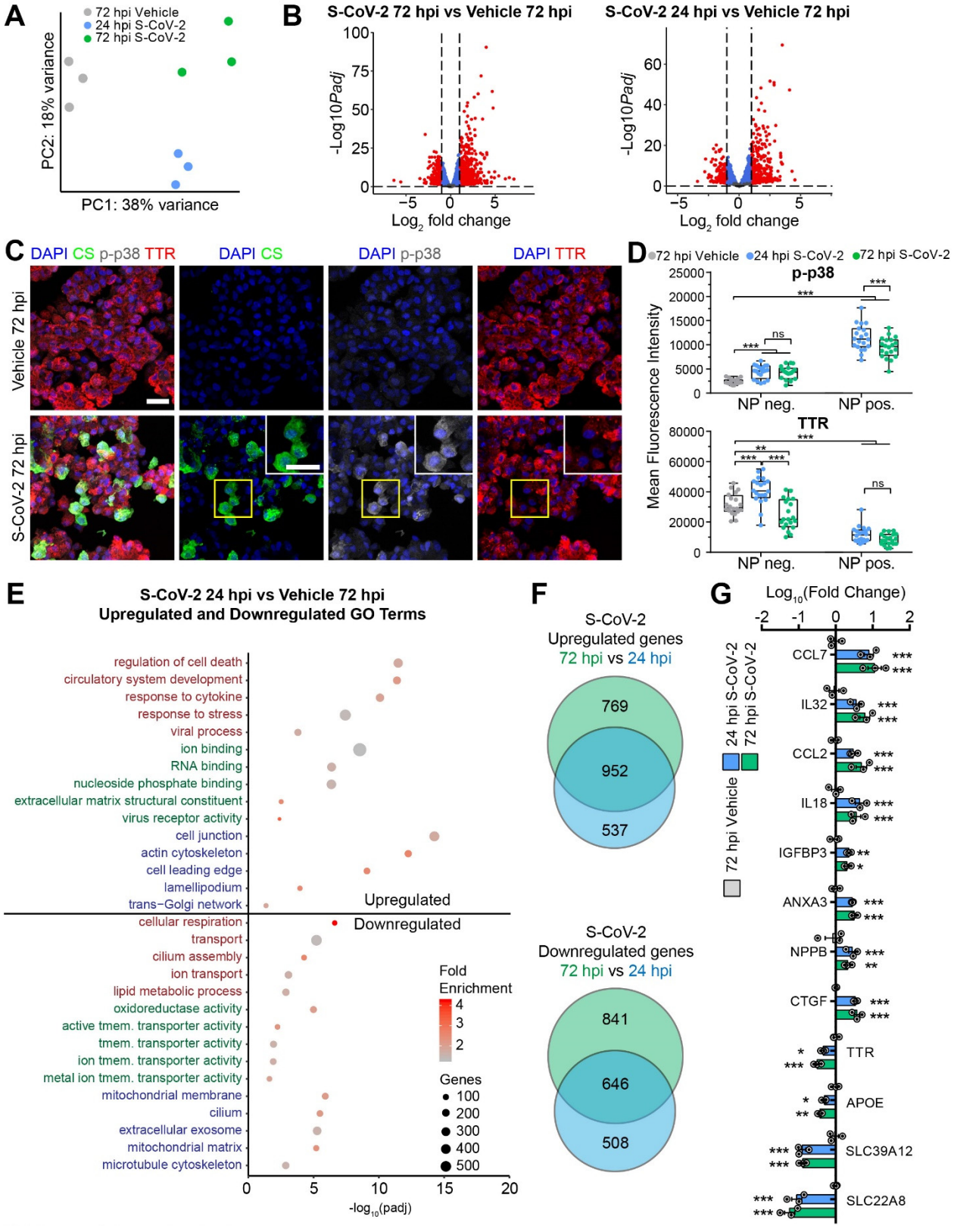

Figure S4. Additional analysis of transcriptional dysregulation in SARS-CoV-2 Infected Choroid Plexus Organoids, related to Figure 4

(A) Principal component analysis (PCA) plot comparing the bulk RNA transcriptomes after S-CoV-2 (10^5 FFU) or vehicle treatment of 47 DIV CPOs at 24 and 72 hpi. Three biological replicates are shown for each condition.
(B) Volcano plot showing the differentially expressed genes comparing 10^5 FFU S-CoV-2-treated and vehicle-treated 47 DIV CPOs at 72 hpi (left) and comparing 10^5 FFU S-CoV-2-treated 47 DIV CPOs at 24 hpi and vehicle-treated CPOs at 72 hpi (right). The gene expression data for 3 biological replicates for each condition were averaged before comparison. Red dots represent genes with $\log_{2(}$fold change)> |1| and *Padj* < 0.05.
(C) Representative confocal images of fluorescent immunohistology for DAPI, patient convalescent serum (CS), phospho-p38 (p-p38), and TTR after S-CoV-2 (10^5 FFU) or vehicle treatment of 67 DIV CPOs at 72 hpi. Insets highlight the regions within the yellow box. Scale bars, 25 μm.
(D) Quantification of the fluorescent intensity of p-p38 (top) and TTR (bottom) in individual SARS-CoV-2 nucleoprotein (NP)-positive and NP-negative cells after S-CoV-2 (10^5 FFU) or vehicle treatment of 67 DIV CPOs at 24 and 72 hpi. Values are shown as a box and whisker plot with the median and 25-75% interquartile ranges. Vertical lines represent the range with individual data points plotted (n = 20 cells per treatment group; **p < 0.01; ***p < 0.001; ns, not significant, p > 0.05; Fisher's LSD Test).
(E) Dot plot of selected enriched gene ontology (GO) terms for biological process (red), molecular function (green), and cellular component (blue) for upregulated and downregulated genes when comparing 10^5 FFU S-CoV-2-treated CPOs at 24 hpi and vehicle-treated CPOs at 72 hpi. See **Table S2** for the complete list of differentially expressed genes and **Table S3** for the complete list of GO terms for differentially expressed genes. tmem.: transmembrane.
(F) Venn diagrams comparing the overlap of upregulated (top) and downregulated (bottom) genes in 10^5 FFU S-CoV-2-treated CPOs at 24 and 72 hpi compared to the vehicle control.
(G) Quantification by quantitative PCR of Log_{10}(Fold Change) of genes dysregulated after 10^5 FFU S-CoV-2 or vehicle treatment of 47 DIV CPOs at 24 and 72 hpi. Values were normalized to that of the vehicle treatment to calculate the fold change for each gene. Values represent mean ± SEM with individual data points plotted (n = 3 biological replicates; *p < 0.05; **p < 0.01; ***p < 0.001; Fisher's LSD Test).

SUPPLEMENTARY TABLES

Table S1. List of primer sequences used for QPCR, related to Figures 2, S2, 4 and S4.

Table S2. List of differentially expressed genes in choroid plexus organoids upon SARS-CoV-2 infection, related to Figure 4.

Table S3. List of GO terms for differentially expressed genes in choroid plexus organoids upon SARS-CoV-2 infection, related to Figure 4.